

## The 2010 Maule, Chile earthquake: Downdip rupture limit revealed by space geodesy

Xiaopeng Tong,<sup>1</sup> David Sandwell,<sup>1</sup> Karen Luttrell,<sup>1</sup> Benjamin Brooks,<sup>2</sup> Michael Bevis,<sup>3</sup> Masanobu Shimada,<sup>4</sup> James Foster,<sup>2</sup> Robert Smalley Jr.,<sup>5</sup> Hector Parra,<sup>6</sup> Juan Carlos Báez Soto,<sup>7</sup> Mauro Blanco,<sup>8</sup> Eric Kendrick,<sup>3</sup> Jeff Genrich,<sup>9</sup> and Dana J. Caccamise II<sup>3</sup>

Received 14 October 2010; accepted 2 November 2010; published 30 December 2010.

[1] Radar interferometry from the ALOS satellite captured the coseismic ground deformation associated with the 2010 Mw 8.8 Maule, Chile earthquake. The ALOS interferograms reveal a sharp transition in fringe pattern at ~150 km from the trench axis that is diagnostic of the downdip rupture limit of the Maule earthquake. An elastic dislocation model based on ascending and descending ALOS interferograms and 13 near-field 3-component GPS measurements reveals that the coseismic slip decreases more or less linearly from a maximum of 17 m (along-strike average of 6.5 m) at 18 km depth to near zero at 43–48 km depth, quantitatively indicating the downdip limit of the seismogenic zone. The depth at which slip drops to near zero appears to be at the intersection of the subducting plate with the continental Moho. Our model also suggests that the depth where coseismic slip vanishes is nearly uniform along the strike direction for a rupture length of ~600 km. The average coseismic slip vector and the interseismic velocity vector are not parallel, which can be interpreted as a deficit in strike-slip moment release. **Citation:** Tong, X., et al. (2010), The 2010 Maule, Chile earthquake: Downdip rupture limit revealed by space geodesy, *Geophys. Res. Lett.*, 37, L24311, doi:10.1029/2010GL045805.

### 1. Introduction

[2] On February 27, 2010, a magnitude 8.8 earthquake struck off the coast of Maule, Chile. The earthquake occurred on a locked megathrust fault resulting from oblique convergence of the oceanic Nazca plate subducting beneath the continental South American plate at ~6.5 cm/yr [Kendrick et al., 2003]. To date, the Maule event is the fifth largest

earthquake since modern recording began, and the largest in this region since the great magnitude 9.5 Chile earthquake in 1960 [National Earthquake Information Center (NEIC), 2010]. Modern geodetic technologies permit this event to be studied in greater detail than was possible for any previous large earthquake. Studying the downdip limit of seismogenic rupture in relation to the compositional layering of surrounding areas may provide insights into the rheological controls on the earthquake process. Of particular interest in the case of continental subduction zones is the relationship between the downdip limit of stick-slip behavior and the depth of the continental Moho at its intersection with the subduction interface [Oleskevich et al., 1999; Hyndman, 2007].

[3] There are at least four approaches to probing the downdip limit of seismic rupture for subduction thrust earthquakes. The first approach uses the maximum depth of the moderate thrust events along plate interfaces from global teleseismic data. Tichelaar and Ruff [1993] estimated the maximum depth of the seismically coupled zone of the Chile subduction zone to be 36–41 km south of 28°S and 48–53 km north of 28°S. Using a similar approach, Pacheco et al. [1993] suggested that this downdip limit is at 45 km depth in Central Chile. A second approach is to use the interseismic velocity from near-field GPS measurements to infer the downdip limit of the locked zone [Brooks et al., 2003; Bürgmann et al., 2005]. However, with the exceptions of Japan and Cascadia, there are generally not enough GPS stations in convergent plate boundaries to accurately constrain the locking depth. The third approach uses precisely located episodic-tremor-and-slip (ETS) (e.g., in Cascadia, southwest Japan, and Mexico) as a proxy for the downdip extent of the seismogenic zone [Rogers and Dragert, 2003; Schwartz, 2007]. A fourth approach uses geodetic measurements (e.g., GPS and InSAR) to invert for the co-seismic slip distribution on the megathrust and infer the downdip limit of the rupture [Pritchard et al., 2007; Hyndman, 2007]. Here we use nearly complete geodetic coverage from ALOS L-band interferometry (launched January 2006) to resolve the spatial variations in slip for the entire Maule, Chile megathrust zone to a resolution of 40 km or better, and thus provide tight constraints on the depth of this rupture.

### 2. InSAR and GPS Data Analysis

[4] We investigated the crustal deformation produced by the  $M_w$  8.8 Maule, Chile earthquake using interferometric synthetic aperture radar (InSAR) [Massonnet and Feigl, 1998] from the Advanced Land Observatory Satellite

<sup>1</sup>Scripps Institution of Oceanography, University of California, San Diego, La Jolla, California, USA.

<sup>2</sup>School of Ocean and Earth Science and Technology, University of Hawaii, Honolulu, Hawaii, USA.

<sup>3</sup>School of Earth Sciences, Ohio State University, Columbus, Ohio, USA.

<sup>4</sup>Earth Observation Research Center, Japan Aerospace Exploration Agency, Tsukuba, Japan.

<sup>5</sup>Center for Earthquake Research and Information, University of Memphis, Memphis, Tennessee, USA.

<sup>6</sup>Instituto Geográfico Militar Chile, Santiago, Chile.

<sup>7</sup>Departamento de Ciencias Geodésicas y Geomática, Universidad de Concepción, Los Angeles, Chile.

<sup>8</sup>Instituto CEDIAC, Facultad de Ingeniería, Universidad Nacional de Cuyo, Mendoza, Argentina.

<sup>9</sup>Division of Geological and Planetary Sciences, California Institute of Technology, Pasadena, California, USA.

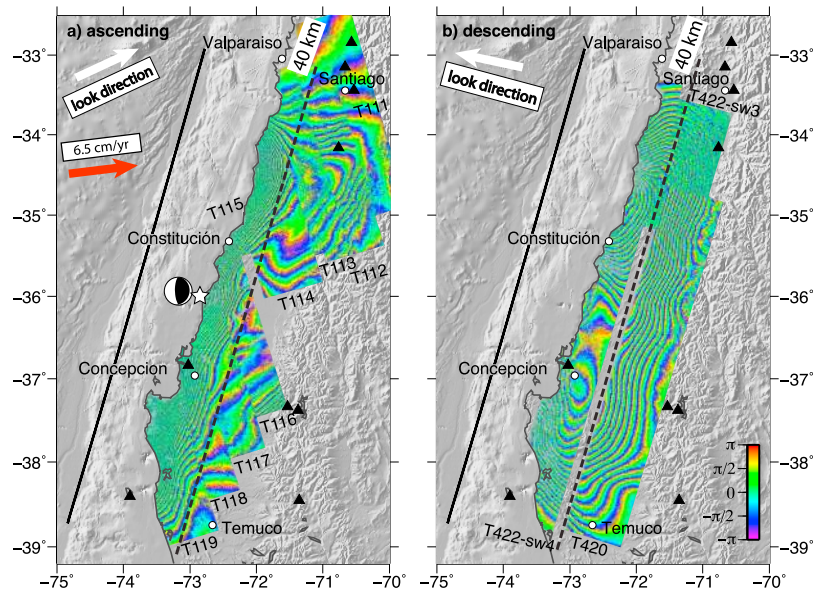


**Figure 1.** (a) Nine tracks of ascending interferograms (FBS-FBS mode) and (b) two tracks of descending interferograms (two subswaths of ScanSAR-ScanSAR mode and ScanSAR-FBS mode, and one track of FBS-FBS mode). The bold white arrow shows the horizontal component of the line of sight look direction. The nominal look angle from the vertical is  $34^\circ$ . The wrapped phase ( $-\pi$  to  $\pi$ ) corresponds a range change of 11.8 cm per cycle). The white star indicates the earthquake epicenter. The black triangles show the locations of the 13 GPS sites used in the inversion (4 sites are outside of the map boundaries). Solid black line shows the surface trace of the simplified fault model and the dashed black line marks the 40-km depth position of the fault for a  $15^\circ$  dip angle. The bold red arrow shows the interseismic convergence vector.

(ALOS) [Shimada *et al.*, 2010] in conjunction with measurements obtained from thirteen continuously operating GPS (CGPS) stations (see auxiliary material).<sup>1</sup> Following the Maule, Chile earthquake, the Japan Aerospace Exploration Agency (JAXA) conducted high priority observations using Fine Beam Single Polarization (FBS) strip-mode SAR along ascending orbits and burst-synchronized ScanSAR along descending orbits. The improved coherence at L-band along with systematic pre- and post-earthquake acquisitions yielded excellent coseismic InSAR coverage of a 630 km by 150 km area of ground deformation (Figure 1). The interferograms were analyzed frame-by-frame using the same local earth radius and spacecraft ephemeris to ensure along-track phase continuity (see Table S2 of the auxiliary material). We used the line-of-sight (LOS) displacement from both ascending and descending orbits to distinguish between horizontal and vertical deformation. We processed track T422-subswath4 (T422-sw4) using newly developed FBS to ScanSAR software following the algorithm of Ortiz and Zebker [2007] and track T422-subswath3 (T422-sw3) using our ScanSAR-ScanSAR processor, which is part of the GMTSAR software [Sandwell *et al.*, 2008; Tong *et al.*, 2010]. The ScanSAR to strip mode interferograms along track T422-sw4 are critical for recovering the complicated deformation near the shoreline from the descending orbits.

[5] An examination of the raw phase data reveals an interesting feature in the coseismic surface deformation: the dashed black line on the ascending interferograms (Figure 1a) marks a boundary where the phase gradient changes remarkably, reflecting that the coseismic slip stopped at  $\sim 150$  km from the trench axis (i.e.,  $\sim 40$  km depth for a fault

with  $15^\circ$  dip angle). At a similar distance from the trench, the descending interferograms exhibit a phase minimum (Figure 1b). Both of these features are diagnostic of the surface deformation immediately above the downdip extent of the megathrust [Savage, 1983]. The different signatures seen in the ascending and descending interferograms are due to the difference in the radar LOS vectors.

[6] As interferograms are only able to detect relative movement, GPS vectors are important for providing absolute measurements of displacement and constraining the overall magnitude of slip [Fialko *et al.*, 2001]. Near-field 3-component GPS displacement vectors in this region provide independent constraints on the fault slip model. We did not include GPS measurements that are beyond  $\sim 300$  km from the coast of the Maule, Chile region. Adding the far-field GPS sites should not change the features of our slip model in the depth of 15–45 km because the geometric attenuation would cause all the far-field GPS measurements to be largely sensitive to the long wavelength part of the model. Methods used for unwrapping the interferograms and adjusting the absolute value of range change to the GPS measurements are discussed in the auxiliary material. We found that it was not necessary to remove a ramp from the interferograms in order to achieve the 10 cm uncertainty assigned to the digitized InSAR measurements.

[7] The LOS displacement ranges from 1 cm to 418 cm along ascending orbits (820 data points) and  $-374$  cm to 15 cm along descending orbits (1112 data points). The maximum LOS displacement along the ascending tracks is near the Peninsula in Arauco, Chile while the maximum negative LOS displacement along the descending track is north of Constitución (see Figure S1 of the auxiliary material). Profiles of LOS displacement (Figures S2a and S2b) show that the characteristic inflection points at

<sup>1</sup>Auxiliary materials are available in the HTML. doi:10.1029/2010GL045805.

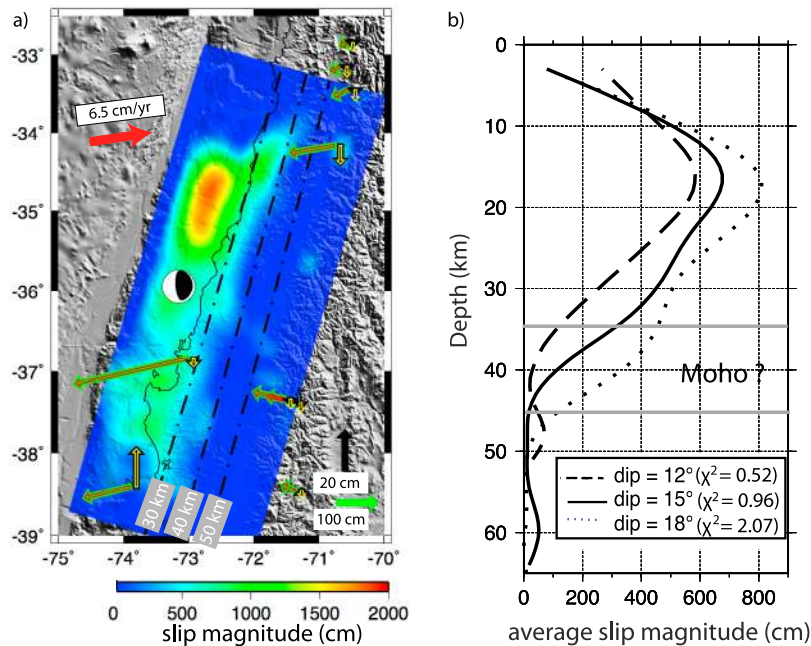


**Figure 2.** (a) Coseismic slip model along a 15° dipping fault plane over shaded topography in Mercator projection. Dashed lines show contours of fault depth. The fat green and black arrows show the observed horizontal and vertical displacement of the GPS vectors respectively and the narrow red and yellow arrows show the predicted horizontal and vertical displacement. (b) Averaged slip versus depth for different dip angles. Data misfits are shown in the parentheses (see text).

~150 km east of the trench are readily discernable from transects of the InSAR LOS displacement.

### 3. Coseismic Slip Model and Resolution Test

[8] We used InSAR and GPS observations to constrain a model of coseismic slip on a single plane striking N 16.8°E and dipping 15° to the east, approximating the geometry of the megathrust (Figure 2a). We also tested a model that more closely follows the trench axis, but the more complicated model did not improve the RMS misfit. The surface trace and dip angle of the fault plane were initially determined by fitting the locations of  $M > 6.0$  aftershocks [NEIC, 2010] and then refined using the geodetic data. The weighted residual misfit is determined from  $\chi^2 = \frac{1}{N} \sum_{i=1}^N \left( \frac{o_i - m_i}{\sigma_i} \right)^2$ , where  $o_i$  is the geodetic displacement measurement,  $m_i$  is the modeled displacement,  $\sigma_i$  is the uncertainty estimate of the  $i^{\text{th}}$  measurement, and  $N$  is the total number of InSAR LOS displacement and 3-component GPS measurements. A 15° dip is preferred because a steeper dip angle (18°) results in a larger misfit (Figure 2b) and a shallower dip angle (12°) results in unlikely maximum slip at the top edge of the fault plane (i.e., 0 km depth). Moreover, the 12° dipping fault plane lies shallower than both the hypocenter and the  $M > 4$  background seismicity from 1960–2007, whose depths are well constrained in the EHB bulletin [International Seismological Centre, 2009] (Figure S2d).

[9] This finite fault model assumes an isotropic homogeneous elastic half-space [Fialko, 2004; Okada, 1985]. Details of the modeling approach are provided in the auxiliary material. The RMS misfit for ascending and descending LOS displacement is 10.9 cm and 7.9 cm respectively and the RMS misfit for the GPS data is: 1.54 cm for the east com-

ponent, 0.44 cm for the north component and 2.93 cm for the up component. The residuals in InSAR LOS displacement (see Figures S1c and S1d of the auxiliary material) are generally smaller than 15 cm, though there are larger misfits in the southern end of the rupture area. The ALOS interferograms, LOS data points and slip model are available at [ftp://topex.ucsd.edu/pub/chile\\_eq/](ftp://topex.ucsd.edu/pub/chile_eq/).

[10] The preferred slip model (Figure 2a) shows significant along-strike variation of the fault rupture. The most intense fault slip is found to be about 17 m, located at 120–160 km north of the epicenter. This is consistent with the large LOS displacement over that region seen in the interferograms (Figure 1). To the south of the epicenter near the peninsula in Arauco, Chile is another patch of significant slip. The length of the rupture area of slip greater than one meter is 606 km, compared with 645 km indicated by the aftershock distribution [NEIC, 2010]. Figure 2b shows the depth distribution of fault slip from the geodetic inversion. The peak of the coseismic slip is located offshore and is at ~18 km depth. The depth of maximum slip is slightly shallower than the depth of rupture initiation, given by the PDE catalog as 22 km [NEIC, 2010].

[11] The coseismic slip model from a joint inversion of GPS and InSAR data (Figure 2a) suggests the slip direction is dominantly downdip, with a relatively small component of right-lateral strike slip. Assuming the average shear modulus to be 40 GPa (see auxiliary material), the total moment of the preferred model is  $1.82 \times 10^{22}$  Nm (thrust component:  $1.68 \times 10^{22}$  Nm; right-lateral strike-slip component:  $4.89 \times 10^{21}$  Nm). The total corresponds to moment magnitude 8.77, comparable to the seismic moment magnitude 8.8 [NEIC, 2010]. Because of the lack of observations offshore, the geodetic model probably underestimates the amount of slip at shallower depth, which could explain the



observed moment discrepancy. The above relatively smooth and simple model results in a variance reduction in the geodetic data of 99%.

[12] We compared the direction of the interseismic velocity vector with the direction of the area-averaged coseismic slip vector. A non-parallel interseismic velocity vector and coseismic slip vector would indicate an incomplete moment release of the Maule event. The interseismic velocity from the Nazca-South America Euler vector is oriented at  $27.3^\circ$  counterclockwise from trench perpendicular [Kendrick *et al.*, 2003]. Based on the ratio of the thrust and right-lateral strike-slip moments, the area-averaged coseismic slip direction is  $16.8^\circ$  counterclockwise from trench perpendicular. The misalignment of the interseismic velocity vector and the coseismic slip vector could be interpreted as a moment deficit in right-lateral strike-slip moment. This moment deficit is about  $3.49 \times 10^{21}$  Nm, equivalent to 70% of the moment release in strike-slip component, which could be accommodated by either aseismic slip or subsequent earthquakes.

[13] The most intriguing observation from the slip model is that the along-strike-averaged slip decreases by more than a factor of 10 between 18 km and 43 km depth and reaches a minimum of approximately zero at a depth of 43–48 km (Figure 2b). This dramatic decrease indicates the downdip limit of the seismogenic zone and the transition from seismic to aseismic slip. In addition we note a depth range where the coseismic slip deviates from a linear decrease and somewhat flattens at 30–35 km depth. This deviation at 30–35 km depth resembles the “plateau” of the interseismic coupling at Nakai Trough, Japan [Aoki and Scholz, 2003]. The depth at which slip drops to near zero is almost uniform in the along-strike direction for a rupture length of  $\sim 600$  km. This depth approximately corresponds to the intersection of the subducting plate with the continental Moho. Based on receiver function and seismic refraction analysis, the Moho depth is between 35 and 45 km [Yuan *et al.*, 2002; Sick *et al.*, 2006], although it is not well resolved at its intersection with the subducting plate.

[14] We used a checkerboard resolution test to explore the model resolution (see auxiliary material) and found that features of 40 km by 40 km are well resolved over the area of InSAR coverage, which provides approximately 10 km absolute depth resolution along the dipping fault plane (see Figure 2b). Slip uncertainties are larger at the top and bottom ends of the fault plane (depth  $< 15$  km and depth  $> 50$  km). The slip model also shows a slight increase in slip at depth greater than 50 km, but this feature is not supported by the resolution analysis.

#### 4. Discussion and Conclusions

[15] We compared the coseismic slip model derived from near-field displacement measurements from this study with previous published slip models. Our geodetic inversion, a teleseismic inversion of P, SH, and Rayleigh wave [Lay *et al.*, 2010] and a joint inversion of InSAR, GPS, and teleseismic data [Delouis *et al.*, 2010] all suggest that the largest slip occurred to the north of the epicenter. However, none of the previous studies have used the InSAR observations from both the ascending and descending orbits to resolve the downdip rupture limit. Our study is novel in that we infer the downdip rupture limit from a prominent change in LOS displacement manifested in interferograms (Figure 1).

[16] The along-strike averaged slip depth distribution suggests that the coseismic slip of the Maule event peaks at 18 km depth and decreases to near zero at 43–48 km depth. From a phenomenological perspective the slip distribution indicates that the contact between oceanic and continental crust is velocity weakening. The largest fraction of interseismic coupling occurs at a depth of  $\sim 18$  km and this fraction decreases more or less linearly with increasing depth to  $\sim 43$  km where it becomes essentially zero. This observation is in fair agreement with the observation that earthquake depth distribution tapers smoothly to zero [Tichelaar and Ruff, 1993; Pacheco *et al.*, 1993], indicating the accumulated and released energy on the megathrust is not a simple step function that goes to zero at 43 km.

[17] Based on available seismic evidence on the local Moho depth, we note that the downdip coseismic rupture limit is near the depth where the subducting Nazca plate intersects with the continental Moho of the South America plate. This downdip limit approximately coincides with the transition in topography from Coast Range to Longitudinal Valley. It is noticeable that the free-air gravity changes from positive to negative at similar location as this downdip limit (see Figure S2c).

[18] There are two possible physical mechanisms controlling the downdip limit of the seismogenic zone. First, fault friction behavior may transition from velocity weakening to velocity strengthening at the depth of the 350–450°C isotherm [Oleskevich *et al.*, 1999; Hyndman, 2007; Klingelhoefer *et al.*, 2010]. Second, the downdip rupture limit may occur at the depth of the fore-arc Moho due to a change in frictional properties associated with the serpentinization of the mantle wedge [Bostock *et al.*, 2002; Hippchen and Hyndman, 2008]. In southern Chile, the 350°C isotherm is at a similar depth as the fore-arc Moho, hence previous studies could not distinguish between the two possible controlling mechanisms [Oleskevich *et al.*, 1999]. The observed monotonic decrease in slip with depth combined with the tapering of the earthquake depth distribution provides new information that can be used to constrain earthquake cycle models at megathrusts. This transitional behavior is similar to what is observed on continental transform faults both in terms of coseismic slip [Fialko *et al.*, 2005] and seismicity [Marone and Scholz, 1988].

[19] In summary we have found: (1) The ALOS interferograms show pronounced changes in fringe pattern at a distance of  $\sim 150$  km from the trench axis that are diagnostic of the downdip rupture limit of the Maule earthquake. (2) An elastic dislocation model based on InSAR and GPS displacement measurements shows that the coseismic slip decreases more or less linearly from its maximum at  $\sim 18$  km depth to near zero at  $\sim 43$  km depth. (3) The depth at which slip drops to near zero is almost uniform in the along-strike direction for a rupture length of  $\sim 600$  km and it appears to be at the intersection of the subducting plate with the continental Moho. (4) The average coseismic slip vector and the interseismic velocity vector are not parallel, suggesting a possible deficit in strike-slip moment release.

[20] **Acknowledgments.** This work is supported by the National Science Foundation Geophysics Program (EAR 0811772) and the NASA Geodetic Imaging Program (NNX09AD12G). Research for this project at the Caltech Tectonic Observatory was supported by the Gordon and Betty Moore Foundation.

## References

- Aoki, Y., and C. H. Scholz (2003), Interseismic deformation at the Nankai subduction zone and the Median Tectonic Line, southwest Japan, *J. Geophys. Res.*, *108*(B10), 2470, doi:10.1029/2003JB002441.
- Bostock, M. G., et al. (2002), An inverted continental Moho and serpentinization of the forearc mantle, *Nature*, *417*, 536–538, doi:10.1038/417536a.
- Brooks, B. A., M. Bevis, R. Smalley Jr., E. Kendrick, R. Manceda, E. Lauria, R. Maturana, and M. Araujo (2003), Crustal motion in the Southern Andes (26°–36°S): Do the Andes behave like a microplate?, *Geochem. Geophys. Geosyst.*, *4*(10), 1085, doi:10.1029/2003GC000505.
- Bürgmann, R., M. G. Kogan, G. M. Steblov, G. Hilley, V. E. Levin, and E. Apel (2005), Interseismic coupling and asperity distribution along the Kamchatka subduction zone, *J. Geophys. Res.*, *110*, B07405, doi:10.1029/2005JB003648.
- Delouis, B., J.-M. Nocquet, and M. Vallée (2010), Slip distribution of the February 27, 2010 Mw = 8.8 Maule earthquake, central Chile, from static and high-rate GPS, InSAR, and broadband teleseismic data, *Geophys. Res. Lett.*, *37*, L17305, doi:10.1029/2010GL043899.
- Fialko, Y. (2004), Probing the mechanical properties of seismically active crust with space geodesy: Study of the coseismic deformation due to the 1992 M(w)7.3 Landers (southern California) earthquake, *J. Geophys. Res.*, *109*, B03307, doi:10.1029/2003JB002756.
- Fialko, Y., M. Simons, and D. Agnew (2001), The complete (3-D) surface displacement field in the epicentral area of the 1999 M(w)7.1 Hector Mine earthquake, California, from space geodetic observations, *Geophys. Res. Lett.*, *28*(16), 3063–3066, doi:10.1029/2001GL013174.
- Fialko, Y., et al. (2005), Three-dimensional deformation caused by the Bam, Iran, earthquake and the origin of shallow slip deficit, *Nature*, *435*, 295–299, doi:10.1038/nature03425.
- Hippchen, S., and R. D. Hyndman (2008), Thermal and structural models of the Sumatra subduction zone: Implications for the megathrust seismogenic zone, *J. Geophys. Res.*, *113*, B12103, doi:10.1029/2008JB005698.
- Hyndman, R. D. (2007), The seismogenic zone of subduction thrust faults: What we know and don't know, in *The Seismogenic Zone of Subduction Thrust Faults*, edited by T. H. Dixon and J. C. Moore, pp. 15–35, Columbia Univ. Press, New York.
- International Seismological Centre (2009), EHB Bulletin, Int. Seismol. Cent., Thatcham, U. K. (Available at <http://www.isc.ac.uk>)
- Kendrick, E., et al. (2003), The Nazca–South America Euler vector and its rate of change, *J. South Am. Earth Sci.*, *16*(2), 125–131, doi:10.1016/S0895-9811(03)00028-2.
- Klingelhoefer, F., M.-A. Gutscher, S. Ladage, J.-X. Dessa, D. Graindorge, D. Franke, C. André, H. Permana, T. Yudistira, and A. Chauhan (2010), Limits of the seismogenic zone in the epicentral region of the 26 December 2004 great Sumatra–Andaman earthquake: Results from seismic refraction and wide-angle reflection surveys and thermal modeling, *J. Geophys. Res.*, *115*, B01304, doi:10.1029/2009JB006569.
- Lay, T., C. J. Ammon, H. Kanamori, K. D. Koper, O. Sufri, and A. R. Hutko (2010), Teleseismic inversion for rupture process of the 27 February 2010 Chile (Mw 8.8) earthquake, *Geophys. Res. Lett.*, *37*, L13301, doi:10.1029/2010GL043379.
- Marone, C., and C. H. Scholz (1988), The depth of seismic faulting and the upper transition from stable to unstable slip regimes, *Geophys. Res. Lett.*, *15*, 621–624, doi:10.1029/GL015i006p00621.
- Massonnet, D., and K. L. Feigl (1998), Radar interferometry and its application to changes in the earth's surface, *Rev. Geophys.*, *36*(4), 441–500, doi:10.1029/97RG03139.
- National Earthquake Information Center (NEIC) (2010), Magnitude 8.8—Offshore Maule, Chile, U. S. Geol. Surv., Denver, Colo. (Available at <http://earthquake.usgs.gov/earthquakes/recenteqsww/Quakes/us201010tfan.php>)
- Okada, Y. (1985), Surface deformation due to shear and tensile faults in a half-space, *Bull. Seismol. Soc. Am.*, *75*(4), 1135–1154.
- Oleskevich, D., R. D. Hyndman, and K. Wang (1999), The updip and downdip limits of subduction earthquakes: Thermal and structural models of Cascadia, south Alaska, S.W. Japan, and Chile, *J. Geophys. Res.*, *104*, 14,965–14,991, doi:10.1029/1999JB900060.
- Ortiz, A. B., and H. Zebker (2007), ScanSAR-to-stripmap mode interferometry processing using ENVISAT/ASAR data, *IEEE Trans. Geosci. Remote Sens.*, *45*(11), 3468–3480, doi:10.1109/TGRS.2007.895970.
- Pacheco, J. F., L. R. Sykes, and C. H. Scholz (1993), Nature of seismic coupling along simple plate boundaries of the subduction type, *J. Geophys. Res.*, *98*(B8), 14,133–14,159, doi:10.1029/93JB00349.
- Pritchard, M. E., E. O. Norabuena, C. Ji, R. Boroschek, D. Comte, M. Simons, T. H. Dixon, and P. A. Rosen (2007), Geodetic, teleseismic, and strong motion constraints on slip from recent southern Peru subduction zone earthquakes, *J. Geophys. Res.*, *112*, B03307, doi:10.1029/2006JB004294.
- Rogers, G., and H. Dragert (2003), Episodic tremor and slip on the Cascadia subduction zone: The chatter of silent slip, *Science*, *300*(5627), 1942–1943, doi:10.1126/science.1084783.
- Sandwell, D. T., et al. (2008), Accuracy and resolution of ALOS interferometry: Vector deformation maps of the Father's Day intrusion at Kilauea, *IEEE Trans. Geosci. Remote Sens.*, *46*(11), 3524–3534, doi:10.1109/TGRS.2008.2000634.
- Savage, J. C. (1983), A dislocation model of strain accumulation and release at a subduction zone, *J. Geophys. Res.*, *88*(B6), 4984–4996, doi:10.1029/JB088iB06p04984.
- Schwartz, S. Y. (2007), Episodic aseismic slip at plate boundaries, in *The Treatise on Geophysics*, vol. 4, *Earthquake Seismology*, edited by G. Schubert, pp. 445–472, doi:10.1016/B978-044452748-6.00076-6, Elsevier, Amsterdam.
- Shimada, M., T. Tadonoand, and A. Rosenqvist (2010), Advanced Land Observing Satellite (ALOS) and Monitoring Global Environmental Change, *Proc. IEEE*, *98*(5), 780–799, doi:10.1109/JPROC.2009.2033724.
- Sick, C., et al. (2006), Seismic images of accretive and erosive subduction zones from the Chilean margin, in *The Andes*, edited by O. Oncken et al., pp. 147–169, doi:10.1007/978-3-540-48684-8\_7, Springer, Berlin.
- Tichelaar, B. W., and L. J. Ruff (1993), Depth of seismic coupling along subduction zones, *J. Geophys. Res.*, *98*(B2), 2017–2037, doi:10.1029/92JB02045.
- Tong, X., D. T. Sandwell, and Y. Fialko (2010), Coseismic slip model of the 2008 Wenchuan earthquake derived from joint inversion of interferometric synthetic aperture radar, GPS, and field data, *J. Geophys. Res.*, *115*, B04314, doi:10.1029/2009JB006625.
- Yuan, X., S. V. Sobolev, and R. Kind (2002), Moho topography in the central Andes and its geodynamic implications, *Earth Planet. Sci. Lett.*, *199*(3–4), 389–402, doi:10.1016/S0012-821X(02)00589-7.
- J. C. Báez Soto, Departamento de Ciencias Geodésicas y Geomática, Universidad de Concepción, Campus Los Angeles, J. A. Coloma 0201, Los Angeles 445-1032, Chile.
- M. Bevis, D. J. Caccamise II, and E. Kendrick, School of Earth Sciences, Ohio State University, 275 Mendenhall Laboratory, 125 South Oval, Columbus, OH 43210, USA.
- M. Blanco, Instituto CEDIAC, Facultad de Ingeniería, Universidad Nacional de Cuyo, Parque General San Martín, Mendoza 405-5500, Argentina.
- B. Brooks and J. Foster, School of Ocean and Earth Science and Technology, University of Hawaii, 1680 East West Rd., Honolulu, HI 96822, USA.
- J. Genrich, Division of Geological and Planetary Sciences, California Institute of Technology, MC 100-23, 272 South Mudd Laboratory, Pasadena, CA 91125, USA.
- K. Luttrell, D. Sandwell, and X. Tong, Scripps Institution of Oceanography, University of California, San Diego, La Jolla, CA 92093-0225, USA. (ttxxpp@gmail.com)
- H. Parra, Instituto Geográfico Militar Chile, Nueva Santa Isabel 1640, Santiago, Chile.
- M. Shimada, Earth Observation Research Center, Japan Aerospace Exploration Agency, Sengen 2-1-1, Tsukuba, Ibaraki 350-8505, Japan.
- R. Smalley Jr., Center for Earthquake Research and Information, University of Memphis, 3876 Central Ave., Ste. 1, Memphis, TN 38152-3050, USA.